Climate Dynamics (2022) 58:1811–1827
https://doi.org/10.1007/s00382-021-05993-5

Interaction between Arctic sea ice and the Atlantic meridional overturning circulation in a warming climate

Wei Liu[1] · **Alexey Fedorov**[2]

Received: 17 April 2021 / Accepted: 30 September 2021 / Published online: 20 October 2021

Abstract
Tentative evidence suggests that the contraction of Arctic sea ice and the slowdown of the Atlantic meridional overturning circulation (AMOC) may have already started in the 1970 or 1980s, which raises the question of how changes in these two key climate components are connected across different timescales. Here, we investigate two-way interactions between Arctic sea ice and AMOC variations using a broad suite of models and climate simulations, including those from the CMIP5 and CMIP6 datasets. Our analysis of preindustrial simulations suggests that Arctic sea ice loss can drive an AMOC slowdown after a multi-decadal delay primarily through the downstream propagation of positive buoyancy (warm/low salinity) anomalies spreading from the Arctic to the subpolar North Atlantic and suppressing deep convection. The AMOC weakening on the other hand acts to expand Arctic sea ice cover within several years via a reduction in northward oceanic heat transport. Analyzing greenhouse-warming simulations, further we show that these interactions should operate under anthropogenic global warming, affecting future projections for Arctic sea ice and the AMOC.

1 Introduction

A dramatic decline of Arctic sea ice has been observed over the past 4 decades (Stroeve et al. 2007; Parkinson and Cavalieri 2008; Swart et al. 2016; Ding et al. 2017). Historical reconstructions (Titchner and Rayner 2014) provide further evidence for a gradual retreat of Arctic sea ice since the 1950s (Fig. 1a). In parallel, the Atlantic meridional overturning circulation (AMOC) has weakened over the past decade as observed at 26° N by the RAPID array (Frajka-Williams 2015; Smeed et al. 2018). Although the robustness of this decadal decline of the AMOC remains unclear given the natural variability in climate system (Robert et al. 2014), temperature-based reconstructions (Rahmstorf et al. 2015; Sévellec et al. 2017) and geochemical proxy reconstructions (Thornalley et al. 2018) of AMOC strength indicate a gradual AMOC weakening since the middle-to-late 20th century (Fig. 1b). Complementary to these historical records, climate models involved in the Climate Model Intercomparison Projects Phase 5 (CMIP5, cf. Taylor et al. 2012) and Phase 6 (CMIP6, cf. Eyring et al. 2016) also simulate a decline in both Arctic sea ice (Fig. 1a) and AMOC strength that started in the late 20th century (Fig. 1b).

It is noteworthy that unlike CMIP5 models, CMIP6 models simulate an AMOC strengthening trend until the mid-1980s, which results from a stronger anthropogenic aerosol forcing on average in CMIP6 as more models in this dataset include aerosol-cloud interactions (Menary et al. 2020; Hassen et al. 2021). Nevertheless, observational constraints suggest that this anthropogenic forcing and/or the AMOC response may be overestimated in the CMIP6 historical simulations (Menary et al. 2020). Despite these differences, both CMIP5 and CMIP6 models predict a further AMOC slowdown during the 21st century under the representative concentration pathway 8.5 (RCP 8.5) and the shared socioeconomic pathway 5-85 (SSP5-85) scenarios, respectively (Fig. 1). Likewise, these models predict a continuing decline of Arctic sea ice area.

The concurrent decline of Arctic sea ice and the AMOC, however, makes their relationship under anthropogenic forcing difficult to disentangle. Nevertheless, some aspects of this relationship have been explored under natural radiative forcing induced by volcanic eruptions (Robock and Mao 1992; Stenchikov et al. 2009; Swingedouw et al. 2017) and/

✉ Wei Liu
wei.liu@ucr.edu

[1] Department of Earth and Planetary Sciences, University of California Riverside, 900 University Ave, Riverside, CA 92501, USA

[2] Department of Earth and Planetary Sciences, Yale University, New Haven, CT, USA

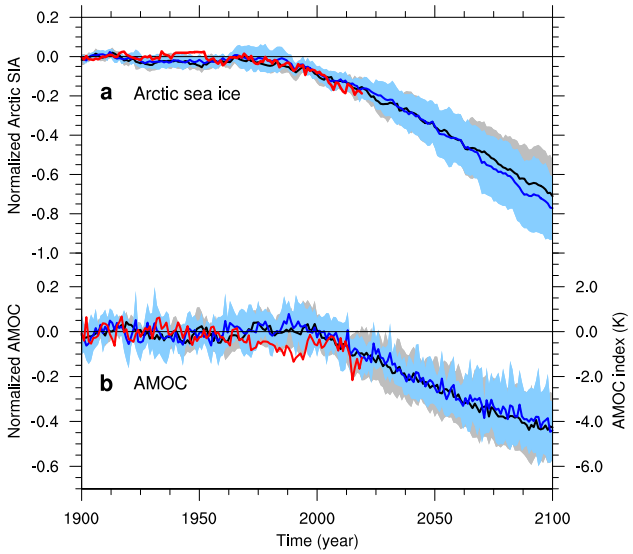

Fig. 1 **a** Annual mean Arctic sea ice area (SIA) anomalies from the HadISST.2 historical reconstruction (red), from the historical and RCP8.5 simulations of 7 CMIP5 models plus CESM1-CAM5-BGC (multi-model mean, i.e. MMM, black), and from the historical and SSP5-85 simulations of 7 CMIP6 models (MMM, blue). **b** Annual mean anomalies of a temperature-based AMOC index based on the NASA GISTEMP v4 data (red) and modeled anomalies of the AMOC strength from historical and RCP8.5 simulations of 7 CMIP5 models plus CESM1-CAM5-BGC (MMM, black), and from historical and SSP5-85 simulations of 7 CMIP6 models (MMM, blue). Anomalies are relative to a 1900–1919 average. Except those of the temperature-based AMOC index, anomalies are further normalized by the 1900–1919 average. Only one (the first) ensemble member from each model's simulations is adopted to ensure an equal weight for individual models. Gray and light blue shadings indicate one standard deviation from the MMMs for the two groups: CMIP5 models plus CESM1-CAM5-BGC and CMIP6 models

or in past climates (Zhong et al. 2011; Lehner et al. 2013; Schleussner and Feulner 2013; Swingedouw et al. 2015; Slawinska et al. 2018; Sadatzki et al. 2019; Halloran et al. 2020). For example, during the last glacial period, sea ice variations in the Nordic Seas were suggested to interact with ocean circulations in the North Atlantic, including the AMOC, as part of the Dansgaard-Oeschger (D-O) cycle (Sadatzki et al. 2019).

During the last millennium, large volcanic eruptions were suggested to increase sea ice export and the related freshwater transport to the North Atlantic deep convection regions, thus diminishing the strength of the AMOC and associated oceanic heat transport to the Arctic, which in turn helps sustain Arctic sea ice expansion (Halloran et al. 2020). This positive feedback was invoked in Lehner et al. (2013) and Schleussner and Feulner (2013) to explain the onset of the Little Ice Age. On the other hand, other studies of ocean response to volcanic eruptions argued that this sea ice expansion was driven by Arctic Ocean cooling, while the reduced poleward oceanic heat transport was primarily due to the advection of anomalously cold water from the subpolar North Atlantic rather than the weaker inflow of the AMOC (Zhong et al. 2011). Yet, other studies showed that, instead of a weakened AMOC, an intensified AMOC developed roughly one decade after strong volcanic eruptions (Swingedouw et al. 2015), which is then followed by a centennial-scale increase of Arctic sea ice cover (Slawinska et al. 2018). Thus, the full relationship between the AMOC and Arctic sea ice in the context of volcanic eruptions remains ambiguous. The interplay between the external, volcanically induced forcing and climate internal variability further complicates the matters.

Studies focusing on modern climate have shown that the AMOC can affect Arctic sea ice (Delworth et al. 2016), especially summer sea ice (Zhang 2015), potentially through the Atlantic Multidecadal Oscillation (Polyakov et al. 2003; Frankcombe et al. 2010; Drinkwater et al. 2014). The AMOC intensity and associated poleward oceanic heat transport are significantly anti-correlated with the Arctic sea ice extent (Zhang 2015; Mahajan et al. 2011) and the latter leads the AMOC by 0–3 years (Day et al. 2012). It has been suggested that anomalously strong AMOC-related poleward oceanic heat transport into the Arctic may have contributed to the observed rapid loss of Arctic sea ice during the late 1900s and early 2000s (Yeager et al. 2015) while a weaker AMOC in the late 2000s may have counteracted the impact of anthropogenic global warming and delayed further Arctic sea ice loss (Kay et al. 2011; Liu et al. 2020).

Other studies approached the problem from a different perspective and investigated how variations in Arctic sea ice and associated changes in the Arctic and subarctic ocean can influence the AMOC. Earlier studies examined how variations in freshwater transport from the Arctic (with no particular focus on Arctic sea ice) can produce positive or negative salinity anomalies in the subpolar North Atlantic (Delworth et al. 1997; Zhang and Vallis 2006). Such anomalies affect deep convection and hence the AMOC (Jungclaus et al. 2005).

A more recent adjoint analysis of AMOC sensitivity to buoyancy fluxes in the Arctic together with targeted coupled simulations isolated the effect of Arctic sea ice decline on AMOC slowdown (Sévellec et al. 2017). Both thermal and haline effects due to Arctic sea ice loss were found to be essential for the AMOC slowdown. This mechanism was further analyzed in Liu et al. (2019), Li et al. (2021) and Li and Fedorov (2021) in a series of numerical perturbation experiments imposing Arctic sea ice decline. These authors have shown that Arctic sea ice loss expands the area of open ocean, allowing more solar heat into the ocean (Levermann et al. 2007) and at the same time increasing surface freshwater flux due to the seasonal sea ice melt. On multi-decadal timescales the resultant positive buoyancy (combined thermal

and haline) anomalies spread over to the subpolar North Atlantic, alter the vertical stratification in ocean (Mignot et al. 2007) and cause the AMOC weakening. A number of other studies, using different models and experimental set-ups, also show a multi-decadal AMOC slowdown that follows Arctic sea ice decline but with a broad range of magnitudes of AMOC change (Jahn and Holland 2013; Blackport and Kushner 2016; Oudar et al. 2017; Wang et al. 2018; Sun et al. 2018).

In general, these two paradigms—AMOC variations affect sea ice by modulating poleward oceanic heat transport versus Arctic sea ice variations affect the AMOC by generating upper-ocean buoyancy anomalies—have not been reconciled so far, especially in the context of anthropogenic climate change with the concurrent Arctic sea ice decline and AMOC slowdown, and in terms of separating externally forced signals from natural climate variability. These are the central topics of the present study.

2 Model simulations and methods

2.1 Climate model simulations

We use 16 state-of-art climate models (Table 1) including 7 CMIP5 models and 7 CMIP6 models that have at least 500-year preindustrial control simulations as well as CESM1-CAM5-BGC and CESM1-CN. Despite inter-model differences, these climate models simulate on average reasonable magnitude of natural variability of Arctic sea ice and the AMOC as compared with the Pan-Arctic Ice Ocean Modeling and Assimilation System (PIOMAS, cf. Schweiger et al. 2011) and RAPID array (Smeed et al. 2018) observations (Table 1). Many other CMIP5/6 models were not used either because they have too weak decadal and multi-decadal variability of Arctic sea ice cover and/or the AMOC, or because they have too short control simulations.

For each model, we use a 500-year output of the preindustrial control simulation in which the radiative forcing due to greenhouse gases, aerosols, ozone, and solar irradiance is fixed at the preindustrial level. As we focus on low-frequency

Table 1 Climate models and simulations used in this study, including 14 CMIP5/CMIP6 models, CESM1-CAM5-BGC and CESM1-CN

Model	Lead (year)	SIV std ($\times 10^3$ km^3)	AMOC std (Sv)	CMIP5/6	Historical + rcp85/ssp5-85
ACCESS1-0	83	1.52	1.18	CMIP5	Historical + rcp85
ACCESS-ESM1-5	39	1.69	1.53	CMIP6	Historical + ssp5-85
CCSM4	76	2.10	0.76	CMIP5	Historical + rcp85
CESM1-CAM5-BGC	57	2.16	0.90		Historical + rcp85
CESM1-CN	83	2.02	0.90		
CMCC-CMS	92	1.36	0.72	CMIP5	Historical + rcp85
GFDL-CM3	80	1.36	1.65	CMIP5	Historical + rcp85
GISS-E2-R	40	1.33	1.56	CMIP5	Historical + rcp85
HadGEM3-GC31-LL	53	1.81	0.94	CMIP6	Historical + ssp5-85
IPSL-CM5A-LR	33	2.49	0.83	CMIP5	Historical + rcp85
MIROC-ESM	72	1.15	0.93	CMIP5	Historical + rcp85
MIROC6	81	1.59	1.33	CMIP6	Historical + ssp5-85
MPI-ESM1-2-HR	37	2.33	1.79	CMIP6	Historical + ssp5-85
MPI-ESM1-2-LR	67	1.64	1.90	CMIP6	Historical + ssp5-85
NorESM2-MM	41	2.18	1.06	CMIP6	Historical + ssp5-85
UKESM1-0-LL	84	2.27	0.93	CMIP6	Historical + ssp5-85
Multi-model mean	69	1.81	1.18		

For each model, a 500-year preindustrial simulation is used. Based on individual preindustrial simulations, lag correlations have been calculated between low-frequency annual-mean Arctic sea ice area and AMOC strength. The time shown corresponds to the positive correlation peaks in Fig. 3 when Arctic sea ice leads the AMOC. One standard derivation (std) of annual mean Arctic sea ice volume (SIV) and AMOC strength from model preindustrial simulations is shown to represent the natural variability of Arctic sea ice and the AMOC in models. The multi-model mean is consistent with the observed standard deviation of SIV (1.13×10^3 km^3) estimated from the detrended PIOMAS for 1979–2019 and of AMOC strength (1.83 Sv, 1 Sv = 10^6 m^3/s) estimated from the RAPID array at 26° N for 2004–2016, respectively. In addition, historical (1900–2005) and RCP8.5 (2006–2100) simulations are used for the CMIP5 models and CESM1-CAM5-BGC, and historical (1900–2014) and SSP5-85 (2015–2100) simulations for the CMIP6 models. For each simulation only the first ensemble member is adopted to ensure equal weight among the models

variability of Arctic sea ice and the AMOC, the time series of the Arctic sea ice area and AMOC strength are detrended and processed with a 31-year running mean. We also use the historical (1900–2005) and RCP8.5 (2006–2100) simulations in CMIP5 and CESM1-CAM5-BGC (CESM version 1 with Community Atmosphere Model version 5 physics in atmosphere and biogeochemistry in ocean), and the historical (1900–2014) and SSP5-85 (2015–2100) simulations in CMIP6. We adopt one (the first) ensemble member from each model's simulations to ensure an equal weight for each model in the analysis. In addition, we use large ensemble simulations with CESM1-CAM5-BGC (from the so-called CESM-LE dataset) that follow the historical plus RCP8.5 scenarios. The first member of CESM-LE extends from 1850 to 2100 while the other members cover 1920–2100 and are generated by introducing round-off magnitude perturbations in their atmospheric initial conditions (Kay et al. 2015). The CESM-LE dataset has 40 ensemble members for 1920–2100.

We also use CESM1-CN (the Community Earth System Model version 1 with carbon nitrogen in land) whose atmosphere and land components use a T31 spectral truncation, and ocean and sea ice components use an irregular horizontal grid that is nominal 3° but becomes significantly finer (~ 1°) around Greenland and over the Arctic and subarctic areas (Shields et al. 2012). Starting from the quasi-equilibrated CESM1-CN preindustrial control run, we conduct an ensemble perturbation experiment by diminishing the albedo of bare and ponded sea ice and of snow cover on ice over the Northern Hemisphere oceans in the sea ice model component. Specifically, we modify the standard deviation parameters of bare and ponded sea ice (R_{ice} and R_{pnd}) from 0 to − 2 and lower the single scattering albedo of snow by 10% in all spectral bands (Liu et al. 2019; Liu and Fedorov 2019). This choice of parameters facilitates our perturbation experiment to reasonably replicate the observed Arctic sea ice contraction change since the satellite era, from the perspectives of both spatial distribution and seasonal cycle.

The model used (CESM1-CN) and the experimental setup are generally similar to those in Liu et al. (2019). In the present study we use nine ensemble members for the perturbation experiment that are generated by slightly varying the initial conditions of the model atmosphere component, while only one ensemble member was used in Liu et al. (2019). Here, the ensemble-mean results minimize the effect of internal variability and hence facilitate a better representation of AMOC response to Arctic sea ice change.

2.2 Arctic sea ice and AMOC metrics

We use Arctic sea ice total area as a measure of Arctic sea ice since (1) this metric is independent of model grid and resolution (Eisenman et al. 2011); and (2) it could precisely depict the changes between sea ice and open ocean, which is critical for measuring solar radiation and freshwater fluxes at ocean surface. The observed annual mean Arctic sea ice area is based on HadISST.2 (Hadley Centre Sea Ice and Sea Surface Temperature data set, version 2)—a monthly historical reconstruction on a 1° × 1° grid for 1900–2019 (Titchner and Rayner 2014). The simulated annual mean Arctic sea ice area in CMIP5/6 and CESM-LE simulations is calculated by integrating the product of sea ice concentration and model grid area over the Arctic and adjacent oceans.

In CMIP5/6 and CESM-LE simulations, the AMOC strength is defined as the maximum value of annual mean meridional stream function below 500 m in the North Atlantic. As long-term AMOC observations are not available, we also use an AMOC index defined as the difference in annual mean surface air temperatures between the subpolar North Atlantic (50–60° N and 10–50° W) and the Northern Hemisphere (Rahmstorf et al. 2015; Sévellec et al. 2017). This AMOC index is calculated from the annual mean of NASA (National Aeronautics and Space Administration) GISS (Goddard Institute for Space Studies) Surface Temperature Analysis version 4 (GISTEMP v4) monthly data on a 2° × 2° grid for 1900–2019 (Hansen et al. 2010). However, one should be careful when interpreting this index, especially for the historical period, as the North Atlantic surface temperature can be affected both by oceanic and atmospheric processes.

3 Results

3.1 The two-way interaction between Arctic sea ice and the AMOC

We first investigate the interaction between Arctic sea ice and the AMOC using climate simulations selected from a broad set of climate models, most taken from the CMIP5 and CMIP6 datasets. We start with the preindustrial control simulations in which anthropogenic warming is absent and the low-frequency variability of Arctic sea ice and the AMOC is part of natural climate variability. As discussed next, the timescales under consideration will be critical to the problem as the interaction between Artic sea ice and the AMOC has distinct features on multi-decadal versus interannual timescales.

We find that variations in the annual mean Arctic sea ice area are positively correlated with AMOC variations when the former (Arctic sea ice) leads the latter (the AMOC) for timespans longer than 2 decades. The positive correlation peaks when the AMOC lags by about 7 decades in the multi-model mean (Fig. 2a), or by 3–9 decades for individual models (Table 1; Fig. 3). While the correlation coefficients are relatively low for the multi-model mean,

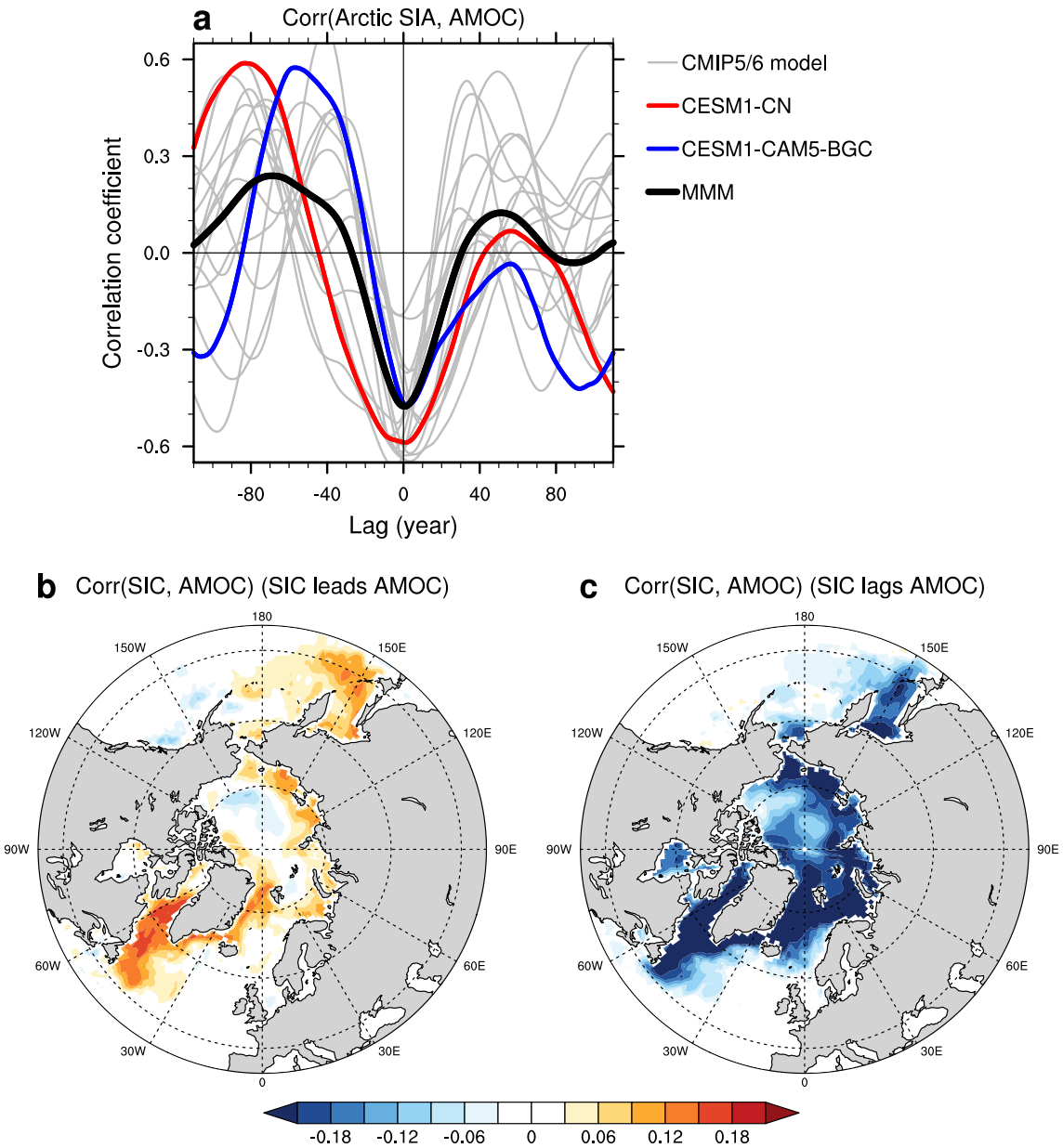

Fig. 2 **a** Lag correlation between annual mean Arctic SIA and AMOC strength in the preindustrial control simulations of 16 climate models (14 CMIP5/6 models, gray; CESM1-CN, red; CESM1-CAM5-BGC, blue; MMM, black). After detrending, a 31-year running mean is applied to both SIA and AMOC time series to isolate low-frequency variability. Positive lags mean that SIA changes lag the AMOC; negative lags mean SIA changes lead the AMOC. Positive correlations at negative lags imply that SIA reduction would lead to AMOC slowdown. **b** A spatial map of the MMM of point correlations between annual mean sea ice concentration (SIC) and AMOC strength at lead periods corresponding to positive correlation peaks (SIC leads the AMOC, Table 1). Note positive correlations at sea ice margins; much larger correlations are seen in individual models. **c** As in **b** but for Arctic sea ice lagging the AMOC by 1 year for all the models

as the best leads vary greatly across the models, the correlations can reach as high as 0.7 for individual models (Fig. 4). Herein the statistical significance of the correlation coefficients accounts for autocorrelation in the time series by using an "effective sample size" (N^*)

$$N^* = N\frac{1 - r_1 r_2}{1 + r_1 r_2} \tag{1}$$

where N is the number of available time steps and r_1 and r_2 are lag-one autocorrelation coefficients of each variable

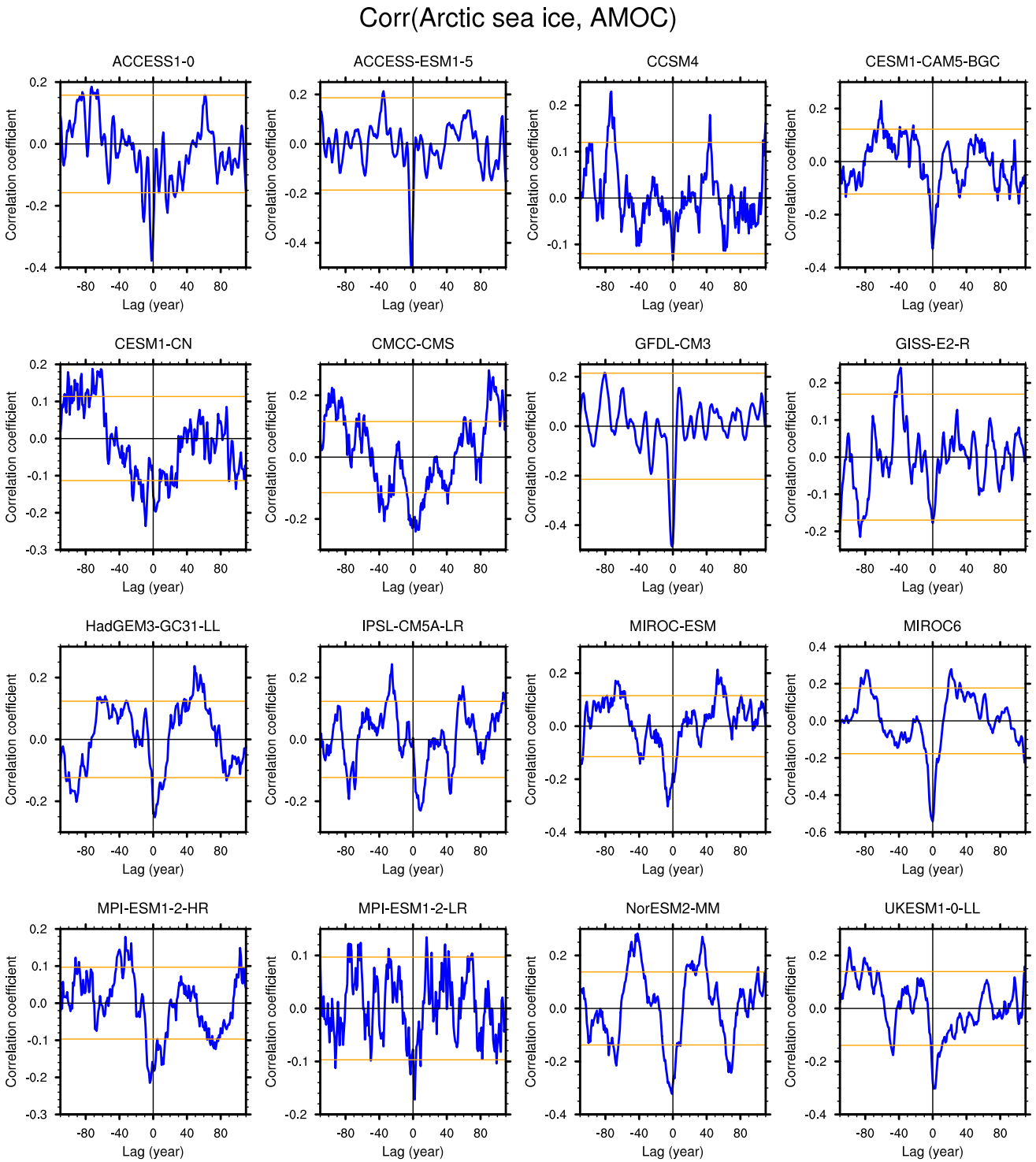

Fig. 3 Lag correlation between annual mean Arctic SIA and AMOC strength in the preindustrial control simulations by different climate models. The time series of Arctic SIA and AMOC strength are detrended. Most models have negative correlations when the SIA lags the AMOC by 0-5 years, and positive correlations when SIA leads the AMOC by 3 to 9 decades. Some models have secondary positive and/or negative peaks suggesting an oscillatory behavior on multi-decadal timescales between the AMOC and Arctic sea ice. Orange lines indicate the 95% significance ($p<0.05$) level based on a two-tailed test. An "effective sample size" is calculated and used to estimate the degrees of freedom in the significance test of correlation

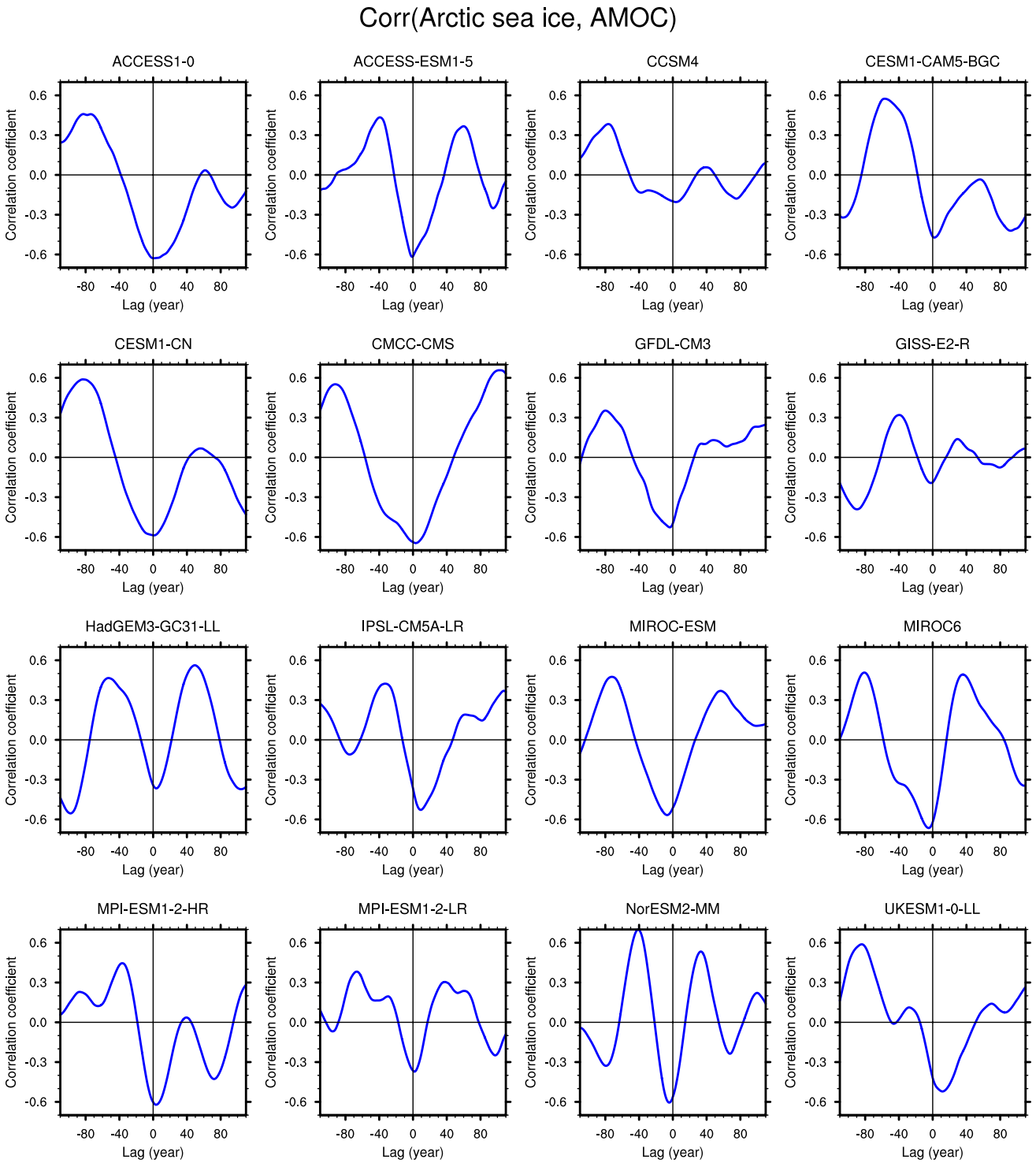

Fig. 4 As in Fig. 3 but with a 31-year running mean applied. The results are shown as gray lines in Fig. 2a

(Bretherton et al. 1999). We examine the significance of the lead-lag correlation between annual mean Arctic sea ice area and AMOC strength in the preindustrial control runs where the time series are detrended but no running mean has been applied (Fig. 3). We find that the peak of positive correlation is significant when Arctic sea ice leads the AMOC by several decades and the peak of negative correlation is significant when Arctic sea ice is in phase with the AMOC or lags the AMOC by a few years (Fig. 3).

One can further examine the spatial pattern of the correlation between sea ice concentration in the Arctic and subarctic areas and the AMOC at the time of correlation peak. Although the details of the pattern differ between the models (Fig. 5), the multi-model mean (Fig. 2b) clearly shows a pattern with positive correlations occurring at the margins

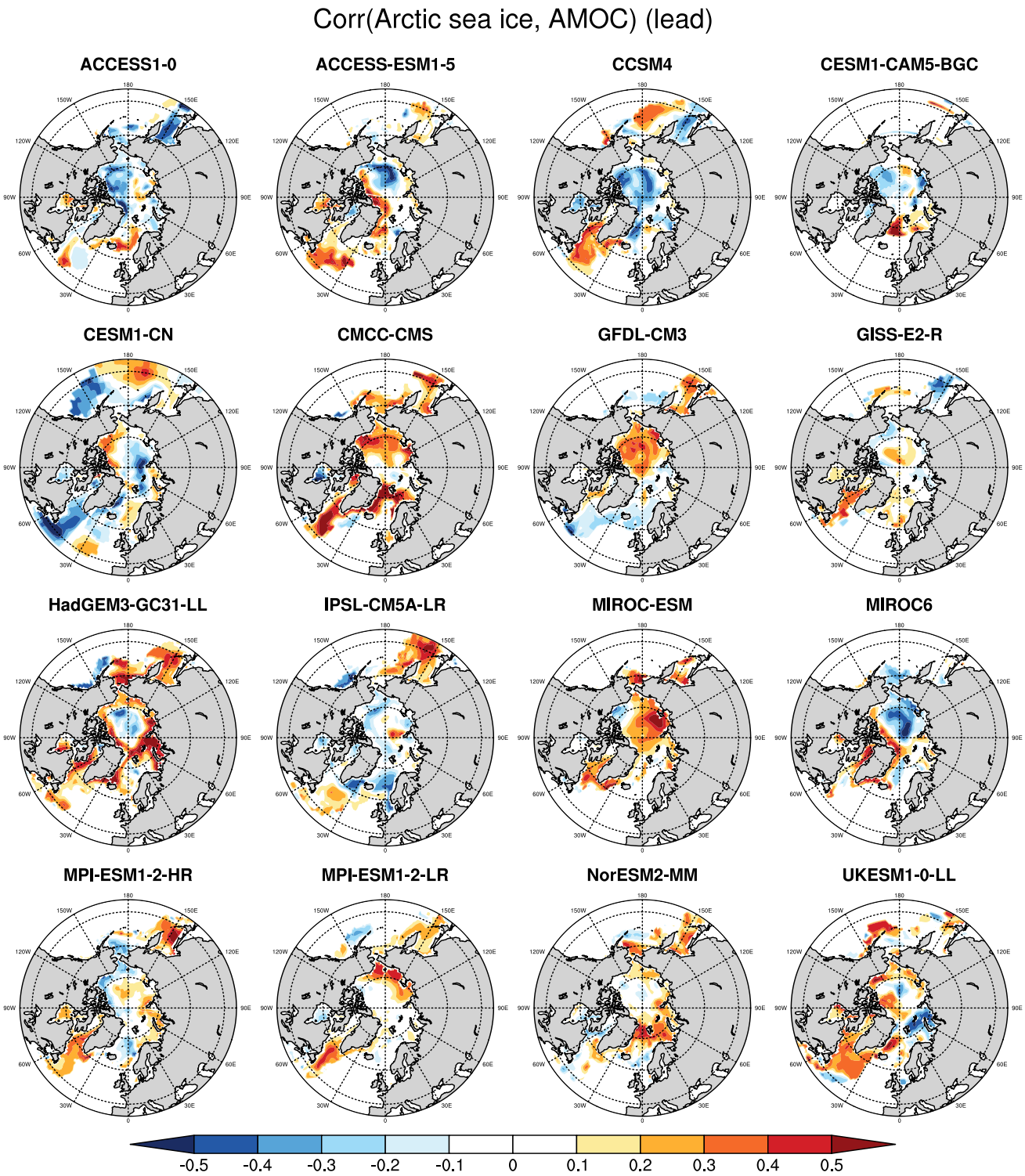

Fig. 5 Spatial maps of correlations between annual mean Arctic sea ice concentration (SIC) and the AMOC strength in the preindustrial control when each model reaches its positive correlation peak (sea ice leads). The time series of SIC and AMOC strength are detrended and a 31-year running mean is applied

of Arctic sea ice, especially in the Labrador Sea, the Nordic Sea and the Bering Sea. This result suggests that on multi-decadal timescales Arctic sea ice retreat can drive an AMOC slowdown, while Arctic sea ice expansion would lead to an AMOC strengthening.

We have also computed the variance of the annual mean Arctic sea ice volume in the 16 models used, which is (3.4 ± 1.5)×10^6 km^6. Applying a 31-year running mean to low-pass decadal or longer variations reduces this value to (1.2 ± 0.6)×10^6 km^6. The ratio between the two variances is (33.1 ± 7.4)%, that is, the low-passed signal explains about one third of the total variance of Arctic sea ice. This multi-decadal and longer variability can sustain the sea ice-AMOC interactions described in this study.

Our correlation analysis is consistent with the previous studies (Sévellec et al. 2017; Liu et al. 2019) that investigated the dynamical mechanism of how changes in Arctic sea ice could drive AMOC changes. We can further illustrate this mechanism by examining the propagation of freshening signals using CESM1-CN experiment wherein the Arctic sea ice albedo was instantaneously reduced. This experiment isolates the effect of Arctic sea ice change while excluding the effect of anthropogenic warming from consideration. We find that the reduced snow/ice albedo causes a rapid Arctic sea ice retreat within the first few years of the simulation (Fig. 6a). Enhanced sea ice melt over the Arctic and sub-arctic ocean induces a strong freshening in the upper ocean, and the signal propagates southward into the North Atlantic (Fig. 7) following the East Greenland Current and the Greenland–Iceland Ridge and Faroe Bank Channel overflows. Together with the warming signals caused by the contraction of sea ice cover (Figs. 6e and 8), these freshening signals in the model reduce seawater density in the upper ocean and suppress deep convection and the North Atlantic Deep Water (NADW) formation in the Nordic Seas and south of Iceland (Figs. 6b and 9).

A Hovmöller diagram of zonal mean salinity anomalies over the Arctic and North Atlantic indicates that the full effect of the freshening will reach the region south of Iceland in about 7 decades after the Arctic sea ice perturbation was imposed (Fig. 6d). Owing to the advection of the signals along the NADW pathways and associated ocean adjustment via wave propagation (Zhang et al. 2010; Sévellec and Fedorov 2013; Muir and Fedorov 2017), AMOC variations in lower latitudes are expected to lag the deep convection changes in the subpolar North Atlantic by several more years. As a result, in this model, the AMOC weakening lags Arctic sea ice loss by about 8 decades (Fig. 6c), which

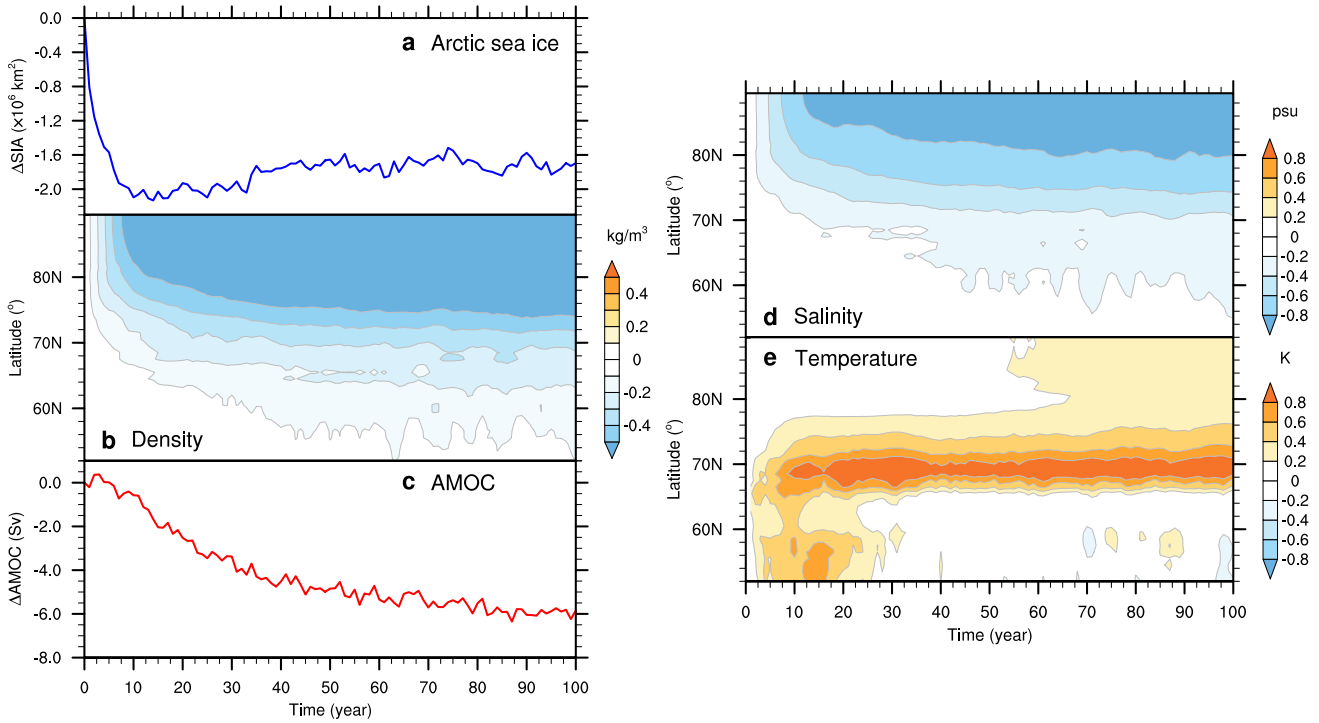

Fig. 6 Results from the Arctic sea ice perturbation experiment: Changes in **a** annual mean Arctic SIA and **c** AMOC strength, and changes in upper-ocean **b** potential density, **d** salinity and **e** temperature over the North Atlantic and Arctic Oceans as a function of time and latitude. The last three variables show zonal mean, upper-ocean 200-m averaged values. These ensemble-mean results are obtained using CESM1-CN. Changes are computed with respect to the annual mean climatology of the model's preindustrial control run. Note that thermal anomalies, important over the deep-convection regions in the first 30 years of the experiment, are then compensated by the reduced northward heat transport of the AMOC

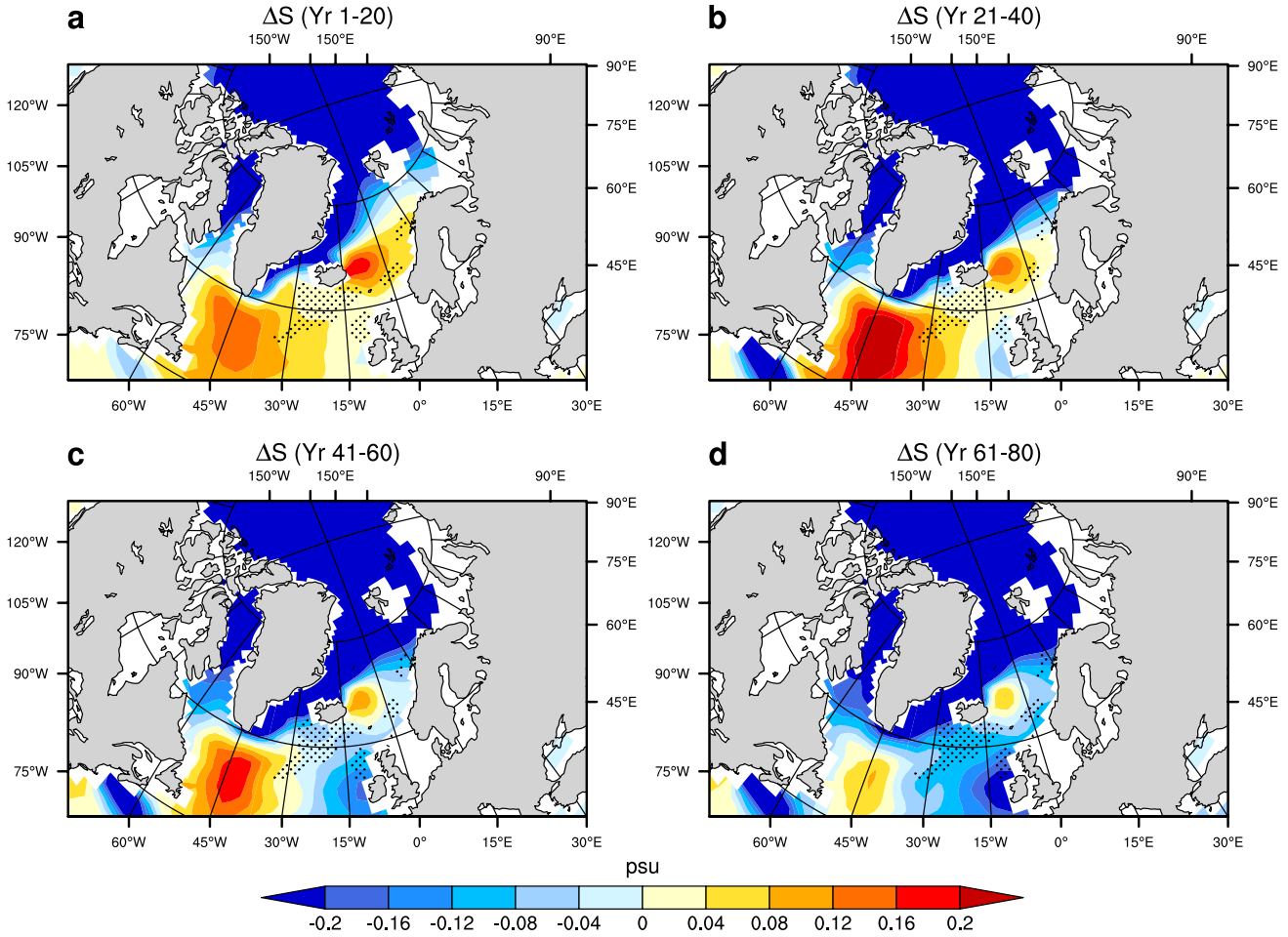

Fig. 7 Annual mean salinity anomalies (color shading; psu) averaged over the upper 200 m for years **a** 1–20, **b** 21–40, **c** 41–60 and **d** 61–80 generated in the CESM1-CN Arctic sea ice albedo perturbation experiment. Ensemble-mean anomalies are shown with respect to the annual mean climatology of the model's preindustrial control run. Stippling marks the model deep convection regions (defined where March mixed layer depth is greater than 400 m)

is consistent with the preindustrial control run indicating that the positive correlation between Arctic sea ice area and the AMOC is maximum when the latter lags the former by about 8 decades (red curve in Fig. 2a). Note however that this effect (i.e. positive correlations) emerges already after around a 40-year lag.

The values of AMOC/Arctic sea ice best lag (Table 1; Fig. 2) depend on the time needed for the buoyancy anomalies to reach the NADW formation regions and for the subsequent ocean adjustment, which shows a large inter-model spread. This spread can be associated with differences in the pattern of Arctic sea ice variability (Semenov et al. 2015), the location and strength of the NADW formation regions (Heuzé 2017), ocean currents in the subpolar North Atlantic (Heuzé and Årthun 2019) and different active modes of AMOC variability (Muir and Fedorov 2017) across climate models. It merits attention that many models display a relatively strong convection in the Labrador Sea (Heuzé 2017), which is influenced by the strength of the North Atlantic subpolar gyre (Born and Stocker 2014). In this context, future studies using observations to evaluate and further constrain models' behavior—for example, deep convection and the NADW formation—could help constrain the timescales of the interactions discussed in this study.

Next, we find that for most models negative correlations develop when Arctic sea ice area lags the AMOC by roughly 0–5 years (Fig. 3). The multi-model mean gives the best lag for negative correlations at about 1 year (Fig. 2a). The spatial pattern of this negative correlation covers most of Arctic sea ice area but is especially pronounced in the Atlantic sector (Figs. 2c and 10). This result confirms the importance of the mechanism discussed by previous studies (Zhang 2015; Mahajan et al. 2011) in which the AMOC affects Arctic sea ice through its poleward oceanic heat transport (a reduction in poleward oceanic heat transport cools high-latitude sea surface temperatures leading to the growth of sea ice). This

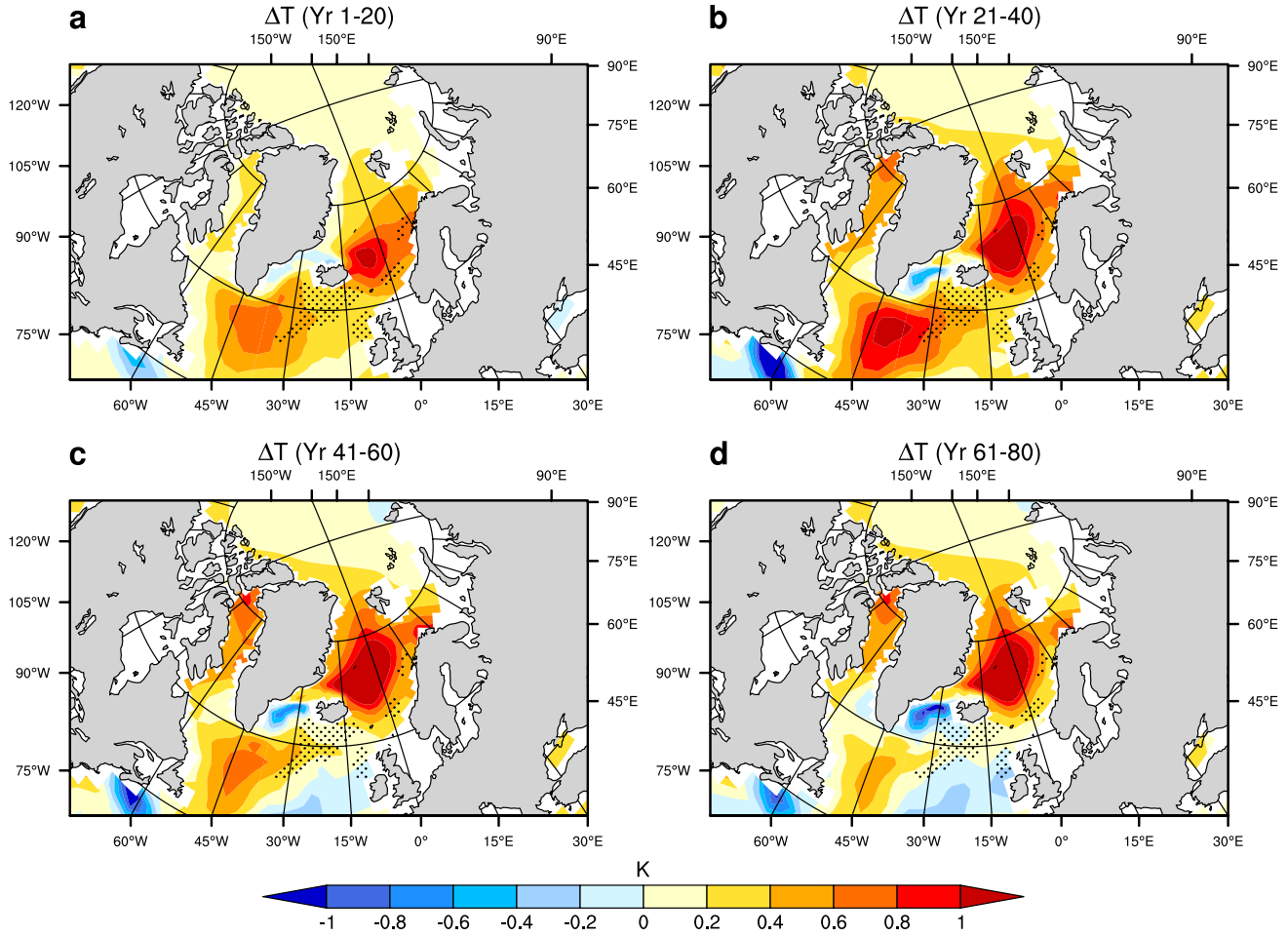

Fig. 8 As in Fig. 7 but for temperature anomalies (color shading; K) averaged over the upper 200 m

mechanism is also present, as a negative feedback, in our perturbation experiment (Fig. 6) wherein sea ice area starts increasing slightly after the first 10 years as the AMOC is weakening. It is worth noting that a strong signal of Arctic sea ice change is also evident in the Sea of Okhotsk, which might be related to atmospheric teleconnections excited by AMOC variations (Liu et al. 2020).

To summarize, our analysis shows that the relationship between Arctic sea ice and the AMOC involves two key mechanisms: sea ice controls the AMOC through buoyancy anomalies while the AMOC controls sea ice via poleward oceanic heat transport. Both mechanisms operate in preindustrial control and sea ice perturbation experiments. They work in opposite directions and involve different timescales. The former mechanism operates on multi-decadal timescales since it takes several decades for sea-ice induced buoyancy anomalies to spread to the North Atlantic and fully affect the AMOC. The latter mechanism operates on a much shorter timescales of several years since a change in AMOC intensity and its poleward oceanic heat transport is felt quite quickly, modulating the Arctic sea ice cover. We also note that in addition to the impacts from Arctic sea ice, the intrinsic dynamics of AMOC interdecadal variability involving mean zonal advection, geostrophic self-advection, and oceanic large-scale baroclinic Rossby waves in the subpolar North Atlantic (e.g., Sévellec and Fedorov 2013, 2015; Muir and Fedorov 2017; Ma et al. 2021) could play a role in this two-way interaction.

3.2 The two-way interaction under global warming

Building on these results, we explore how the two-way interaction between Arctic sea ice and the AMOC may manifest under global warming, subject to anthropogenic forcing and ensuing feedbacks. Here we examine future climate simulations within a large ensemble approach, since all ensemble members experience the same anthropogenic forcing while inter-member differences can reveal the connection between Arctic sea ice and the AMOC. We choose the CESM large ensemble (CESM-LE) based on CESM1-CAM5-BGC that has a large number of members (40 in total) with historical and RCP 8.5 simulations for 1920–2100.

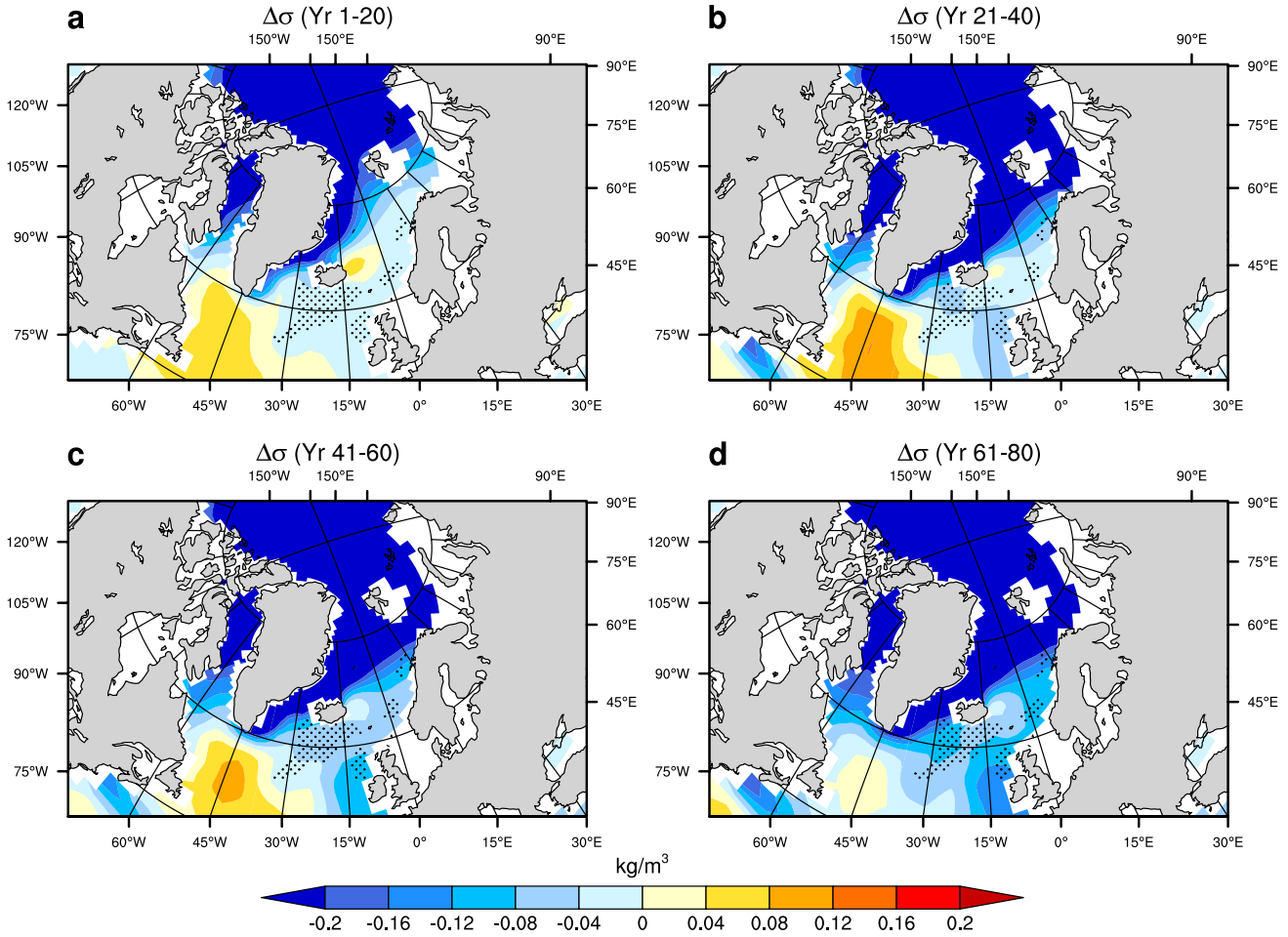

Fig. 9 As in Fig. 7 but for potential density anomalies (color shading; kg/m^3) averaged over the upper 200 m

To examine the relationship between the AMOC and Arctic sea ice within this large ensemble in the context of recent sea ice decline, firstly we estimate for each ensemble member the change of sea ice area in the Arctic for the period 1997–2016 relative to 1920–1939 (**Δ**SIA, 1997–2016 minus 1920–1939). The latter, reference interval is chosen as a representative of near preindustrial conditions. Then we compute the corresponding AMOC changes between similar time intervals but shifted by +64 years and by − 1 year, $\mathbf{\Delta}\mathrm{AMOC}_{\mathrm{lag=64year}}$ (2061–2080 minus 1997–2061) and $\mathbf{\Delta}\mathrm{AMOC}_{\mathrm{lead=1year}}$ (1998–2017 minus 1921–1940), respectively. These time shifts, or the lag and the lead times, are based on the highest positive and negative correlations for this particular model (blue curve in Fig. 2a).

We find that, although the magnitudes of Arctic sea ice loss and AMOC slowdown vary broadly among individual ensemble members, the 40 ensemble members taken together show a significant positive correlation ($r = 0.47$, $p < 0.01$) between changes in Arctic sea ice and future changes in the AMOC (i.e. between **Δ**SIA and $\mathbf{\Delta}\mathrm{AMOC}_{\mathrm{lag=64year}}$, Fig. 11a). In terms of spatial patterns, positive correlations are most robust at sea-ice margins (Fig. 11c), suggesting that a greater Arctic sea ice loss (related to natural variability within ensemble experiments) will drive a stronger future AMOC slowdown in about 6 decades.

We also examine the relationship between the AMOC weakening and Arctic sea ice change measured with 1-year delay (i.e. between **Δ**SIA and $\mathbf{\Delta}\mathrm{AMOC}_{\mathrm{lead=1year}}$, Fig. 11b). We find that the ensemble members show a significant negative correlation ($r = -0.61$, $p < 0.01$) between these changes in the AMOC and Arctic sea ice area, which indicates that an AMOC decline can mitigate Arctic sea ice loss in the coming year by diminishing poleward oceanic heat transport (Fig. 12). Negative correlations appear in most of the Arctic but are especially pronounced in the Atlantic sector (Fig. 11d). This result is consistent with Årthun et al. (2012) and Yeager et al. (2015), discussing the role of the AMOC and associated oceanic heat transport in Arctic sea ice change over the past decades and in the future. It is also worth mentioning that in this study the interaction between Arctic sea ice and the AMOC is examined from the perspective of internal variability of

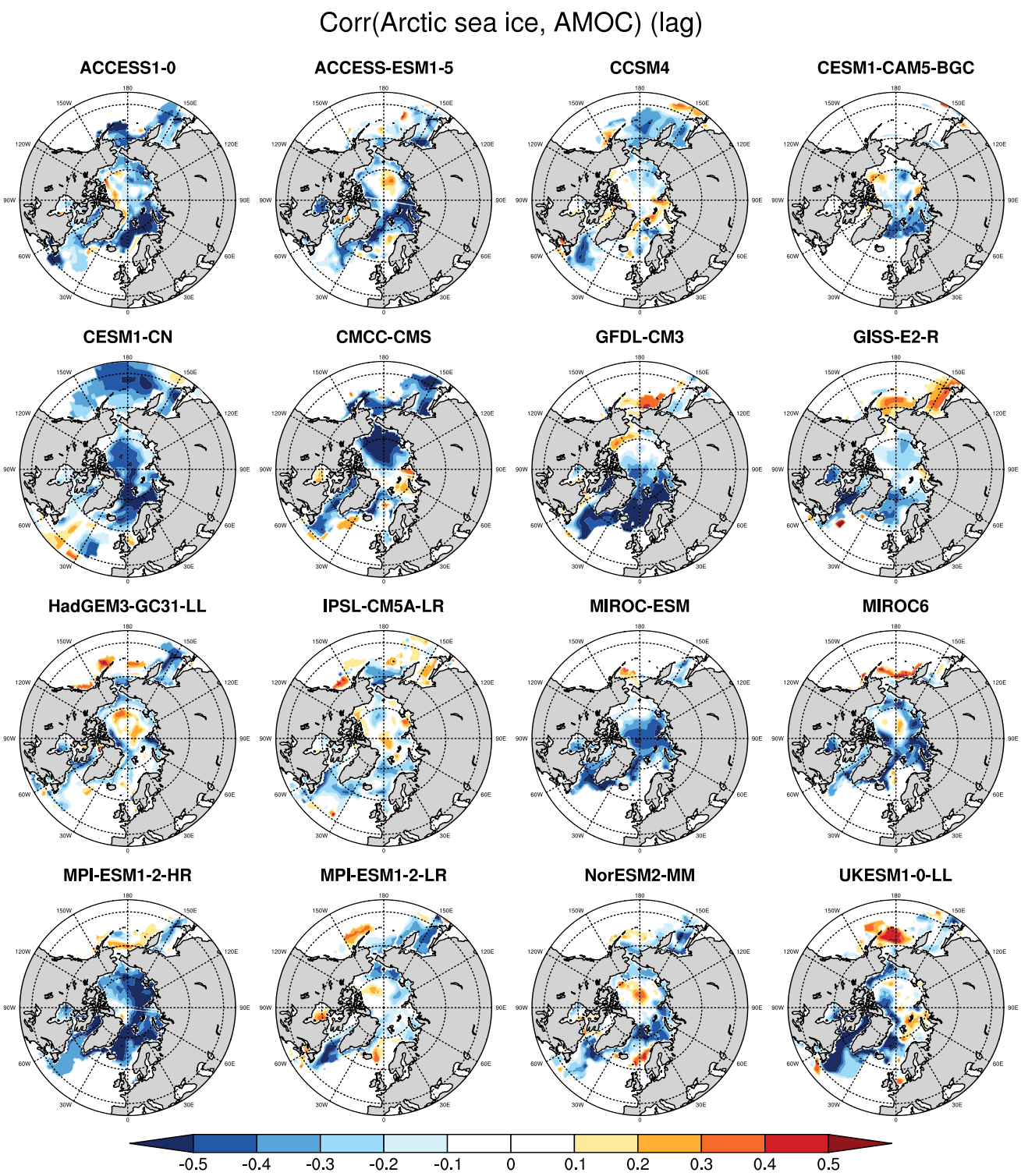

Fig. 10 As in Fig. 5 but when SIC lags the AMOC by 1 year

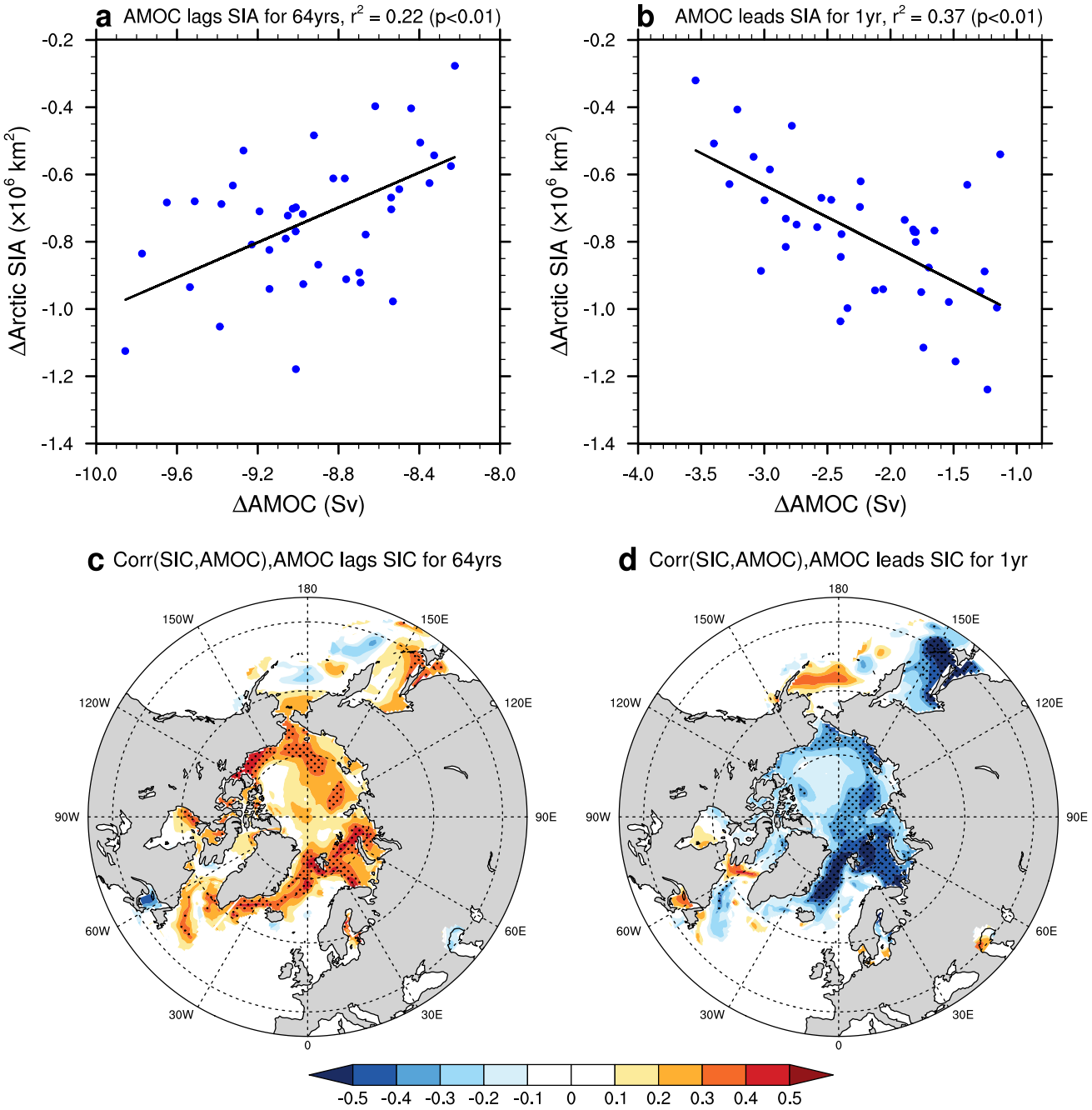

Fig. 11 **a** A scatter plot of annual mean Arctic sea ice area loss (ΔSIA < 0) in 1997–2016 (relative to 1920–1939) and the subsequent AMOC reduction with a shift of 64 years ($\Delta AMOC_{lag=64year}$) in CESM-LE. Blue dots indicate individual ensemble members. The best-fit line (black) is calculated as the first Empirical Orthogonal Function (EOF) mode in the sea ice-AMOC space. For exact definition of anomalies see the text. **b** The same but for **Δ**SIA and $\Delta AMOC_{lead=1year}$. **c**, **d** Spatial maps of point correlations between local changes in annual mean SIC and AMOC strength, corresponding to **a** and **b**, respectively. Stippling in **c** and **d** indicates that the response is statistically significant at the 95% confidence level

two components. In this context, the AMOC change primarily governs the variations of meridional oceanic heat transports that affect Arctic sea ice and potentially Arctic climate (Oldenburg et al. 2018), which is different from the scenarios relying on external forcing (Nummerlin et al. 2017; Oldenburg et al. 2018).

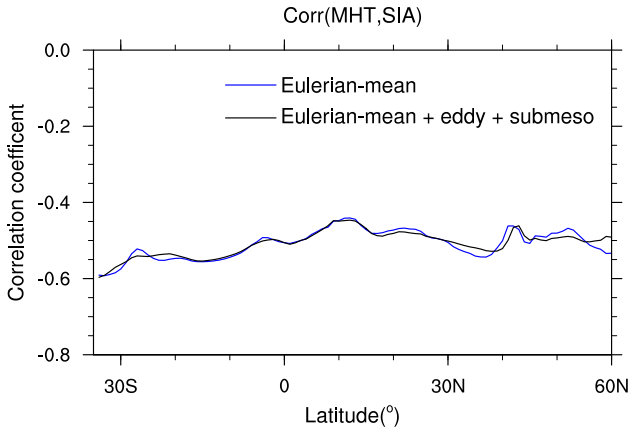

Fig. 12 Correlation between anomalies (relative to the ensemble mean) in the Atlantic meridional heat transport (MHT) difference between two periods (1997–2016 minus 1920–1939) and anomalies in the Arctic SIA difference between the same periods but shifted by 1 year (1998–2017 minus 1921–1940) as a function of latitude in CESM-LE. Blue: MHT is based on Eulerian-mean advection; black: MHT includes Eulerian-mean, eddy-induced and sub-mesoscale advection. The correlation is statistically significant at the 95% confidence level. This plot confirms a significant negative correlation between MHT and SIA decadal changes, with the latter lagging the former by 1 year

4 Conclusions and discussions

We have probed two-way interactions between Arctic sea ice and the AMOC. Using a broad selection of coupled models, we have shown that at multi-decadal lead times (when Arctic sea ice leads by 3 decades or longer) Arctic sea ice decline can drive an AMOC slowdown, whereas at a several-year lag times (when Arctic sea ice lags by ~ 1 year) AMOC slowdown can cause an Arctic sea ice expansion via changes in the associated poleward oceanic heat transport.

Furthermore, as seen in large ensemble climate simulations, the inter-member difference of the simulated recent Arctic sea ice decline is positively correlated with the inter-member difference of projected AMOC slowdown under the RCP8.5 scenario with a lag of the AMOC by about 6 decades, whereas the inter-member difference of recent AMOC weakening is negatively correlated with the inter-member difference of Arctic sea ice loss in the coming year. This result indicates that the two-way interaction between Arctic sea ice and the AMOC can indeed manifest under anthropogenic warming, modulating the AMOC strength and Arctic sea ice cover.

We note that the statistical analysis of our study by itself would not imply causality, especially with the relatively low correlations we see. However, we emphasize that our statistical results are complementary to, and should be considered together with the perturbation model experiments conducted previously by these and other authors on the connections between Arctic sea ice and the AMOC, as well as the experiments presented in the current study.

It is noteworthy that anthropogenic warming could simultaneously affect Arctic sea ice and the AMOC in ways different from the interaction mechanism described here, causing their concurrent evolutions (Arctic sea ice loss and the weakening of the AMOC) under anthropogenic warming. Other processes can contribute to Arctic sea ice loss and AMOC slowdown. In particular, Arctic sea ice loss can come from the changes in large-scale atmospheric circulation (Maslanik et al. 2007; Deser and Tung 2008), low clouds (Francis and Hunter 2006) or oceanic heat transport from the Pacific (Shimada et al. 2006). An AMOC slowdown could be caused by the changes in air-sea heat fluxes and ocean temperature (Gregory et al. 2005; Weaver et al. 2007) and/or freshwater discharge from Greenland Ice Sheet melting and altered hydrological cycle (Hu et al. 2009; Bakker et al. 2016; Ma et al. 2020), further influenced by AMOC stability (Liu and Liu 2013; Liu et al. 2014, 2017). The AMOC can also recover part of its strength under sustained climatic forcing due to the ocean subsurface warming (Thomas and Fedorov 2019).

Additionally, changes in atmospheric circulation, including atmospheric blocking (Drijfhout et al. 2013) and remote effects from other ocean basins (Hu and Fedorov 2019, 2020) can also modulate sea-ice transport and the AMOC. The present study has demonstrated that the Arctic sea ice – AMOC interaction is indeed one of the important mechanisms to consider, especially when predicting future changes in Arctic sea ice and the AMOC.

Acknowledgements W.L. has been supported by the Regents' Faculty Fellowship, by the Alfred P. Sloan. Foundation as a Research Fellow and by US National Science Foundation (AGS-2053121, OCE 2123422). A.V.F. has been supported by grants from the DOE Office of Science (DE-SC0016538), NSF (OCE-1756682, OPP-1741841) and the ARCHANGE project (ANR-18-MPGA-0001, France).

Data availability The HadISST.2 sea ice data are publicly available at https://www.metoffice.gov.uk/hadobs/hadisst2/data/. The NASA GISTEMP v4 data are publicly available at https://data.giss.nasa.gov/gistemp/. The CMIP5/6 data are publicly available through the Earth System Grid Federation (ESGF) https://esgf-node.llnl.gov/projects/esgf-llnl/. The CESM-LE data are publicly available on the Earth System Grid (ESG) https://www.earthsystemgrid.org. The CESM1-CN Arctic sea ice perturbation experiment data are available on request from the corresponding author.

References

Årthun M, Eldevik T, Smedsrud LH, Skagseth Ø, Ingvaldsen RB (2012) Quantifying the influence of Atlantic heat on Barents Sea ice variability and retreat. J Clim 25:4736–4743

Bakker P, Schmittner A, Lenaerts JTM, Abe-Ouchi A, Bi D, van den Broeke MR, Chan WL, Hu A, Beadling RL, Marsland SJ,

Mernild SH (2016) Fate of the Atlantic meridional overturning circulation: strong decline under continued warming and Greenland melting. Geophys Res Lett 43:12252–12260
Born A, Stocker TF (2014) Two stable equilibria of the Atlantic Subpolar Gyre. J Phys Oceanogr 44:246–264
Bretherton CS, Widmann M, Dymnidov VP, Wallace JM, Blade I (1999) The effective number of spatial degrees of freedom of a time-varying field. J Clim 12:1990–2009
Day JJ, Hargreaves JC, Annan JD, Abe-Ouchi A (2012) Sources of multi-decadal variability in Arctic sea ice extent. Environ Res Lett 7:034011
Delworth TL, Manabe S, Stouffer RJ (1997) Multidecadal climate variability in the Greenland Sea and surrounding regions: a coupled model simulation. Geophys Res Lett 24:257–260
Delworth TL, Zeng F, Vecchi GA, Yang X, Zhang L, Zhang R (2016) The North Atlantic Oscillation as a driver of rapid climate change in the Northern Hemisphere. Nat Geosci 9:509–512
Deser C, Teng H (2008) Evolution of Arctic sea ice concentration trends and the role of atmospheric circulation forcing, 1979–2007. Geophys Res Lett 35:L02504
Ding Q, Schweiger A, L'Heureux M, Battisti DS, Po-Chedley S, Johnson NC, Blanchard-Wrigglesworth E, Harnos K, Zhang Q, Eastman R, Steig EJ (2017) Influence of high-latitude atmospheric circulation changes on summertime Arctic sea ice. Nat Clim Change 7:289–295
Drijfhout S, Gleeson E, Dijkstra HA, Livina V (2013) Spontaneous abrupt climate change due to an atmospheric blocking–sea-ice–ocean feedback in an unforced climate model simulation. Proc Natl Acad Sci 110:19713–19718
Drinkwater KF, Miles M, Medhaug I, Otterå OH, Kristiansen T, Sundby S, Gao Y (2014) The Atlantic multidecadal oscillation: its manifestations and impacts with special emphasis on the Atlantic region north of 60° N. J Mar Syst 133:117–130
Eisenman I, Schneider T, Battisti DS, Bitz CM (2011) Consistent changes in the sea ice seasonal cycle in response to global warming. J Clim 24:5325–5335
Eyring V, Bony S, Meehl GA, Senior CA, Stevens B, Stouffer RJ, Taylor KE (2016) Overview of the Coupled Model Intercomparison Project Phase 6 (CMIP6) experimental design and organization. Geosci Model Dev 9:1937–1958
Frajka-Williams E (2015) Estimating the Atlantic overturning at 26° N using satellite altimetry and cable measurements. Geophys Res Lett 42:3458–3464
Francis JA, Hunter E (2006) New insight into the disappearing Arctic sea ice cover. Eos Trans AGU 67:509–511
Frankcombe LM, von der Heydt A, Dijkstra HA (2010) North Atlantic multidecadal climate variability: an investigation of dominant time scales and processes. J Clim 23:3626–3638
Gregory JM, Dixon KW, Stouffer RJ, Weaver AJ, Driesschaert E, Eby M, Fichefet T, Hasumi H, Hu A, Jungclaus JH, Kamenkovich IV (2005) A model intercomparison of changes in the Atlantic thermohaline circulation in response to increasing atmospheric CO_2 concentration. Geophys Res Lett 32:L12703
Halloran PR, Hall IR, Menary M, Reynolds DJ, Scourse JD, Screen JA, Bozzo A, Dunstone N, Phipps S, Schurer AP, Sueyoshi T (2020) Natural drivers of multidecadal Arctic sea ice variability over the last millennium. Sci Rep 10:688
Hansen J, Ruedy R, Sato M, Lo K (2010) Global surface temperature change. Rev Geophys 48:RG4004
Hassan T, Allen RJ, Liu W, Randles CA (2021) Anthropogenic aerosol forcing of the Atlantic meridional overturning circulation and the associated mechanisms in CMIP6 models. Atmos Chem Phys 21:5821–5846
Heuzé C (2017) North Atlantic deep water formation and AMOC in CMIP5 models. Ocean Sci 13:609–622
Heuzé C, Årthun M (2019) The Atlantic inflow across the Greenland–Scotland ridge in global climate models (CMIP5). Elem Sci Anthr 7:16
Hu S, Fedorov AV (2019) Indian Ocean warming can strengthen the Atlantic meridional overturning circulation. Nat Clim Change 9:747–751
Hu S, Fedorov AV (2020) Indian Ocean warming as a driver of the North Atlantic warming hole. Nat Commun 11:1–11
Hu A, Meehl GA, Han W, Yin J (2009) Transient response of the MOC and climate to potential melting of the Greenland ice sheet in the 21st century. Geophys Res Lett 36:L10707
Jahn A, Holland MM (2013) Implications of Arctic sea ice changes for North Atlantic deep convection and the meridional overturning circulation in CCSM4-CMIP5 simulations. Geophys Res Lett 40:1206–1211
Jungclaus JH, Haak H, Latif M, Mikolajewicz U (2005) Arctic–North Atlantic interactions and multidecadal variability of the meridional overturning circulation. J Clim 18:4013–4031
Kay JE, Holland MM, Jahn A (2011) Inter-annual to multi-decadal Arctic sea ice extent trends in a warming world. Geophys Res Lett 38:L15708
Kay JE, Deser C, Phillips A, Mai A, Hannay C, Strand G, Arblaster JM, Bates SC, Danabasoglu G, Edwards J, Holland M (2015) The Community Earth System Model (CESM) large ensemble project: a community resource for studying climate change in the presence of internal climate variability. Bull Am Meteorol Soc 96:1333–1349
Lehner F, Born A, Raible CC, Stocker TF (2013) Amplified inception of European little Ice Age by sea ice-ocean-atmosphere feedbacks. J Clim 26:7586–7602
Levermann A, Mignot J, Nawrath S, Rahmstorf S (2007) The role of northern sea ice cover for the weakening of the thermohaline circulation under global warming. J Clim 20:4160–4171
Li H, Fedorov AV (2021) Persistent freshening of the Arctic Ocean and changes in the North Atlantic salinity caused by Arctic sea ice decline. Clim Dyn. https://doi.org/10.1007/s00382-021-05850-5
Li H, Fedorov AV, Liu W (2021) AMOC stability and diverging response to Arctic sea ice decline in two climate models. J Clim 34:5443–5460
Liu W, Fedorov AV (2019) Global impacts of Arctic sea ice loss mediated by the Atlantic meridional overturning circulation. Geophys Res Lett 46:944–952
Liu W, Liu Z (2013) A diagnostic indicator of the stability of the Atlantic meridional overturning circulation in CCSM3. J Clim 26:1926–1938
Liu W, Liu Z, Brady EC (2014) Why is the AMOC monostable in coupled general circulation models? J Clim 27:2427–2443
Liu W, Xie S-P, Liu Z, Zhu J (2017) Overlooked possibility of a collapsed Atlantic meridional overturning circulation in warming climate. Sci Adv 3:e1601666
Liu W, Fedorov A, Sévellec F (2019) The mechanisms of the Atlantic meridional overturning circulation slowdown induced by Arctic Sea ice decline. J Clim 32:977–996
Liu W, Fedorov AV, Xie S-P, Hu S (2020) Climate impacts of a weakened Atlantic meridional overturning circulation in a warming climate. Sci Adv 6:eaaz4876
Ma X, Liu W, Allen RJ, Huang G, Li X (2020) Dependence of regional ocean heat uptake on anthropogenic warming scenarios. Sci Adv 6:eabc0303
Ma X, Liu W, Burls NJ, Chen C, Cheng J, Huang G, Li X (2021) Evolving AMOC multidecadal variability under different CO_2 forcings. Clim Dyn 57:593–610

Mahajan S, Zhang R, Delworth TL (2011) Impact of the Atlantic Meridional Overturning Circulation (AMOC) on Arctic surface air temperature and sea-ice variability. J Clim 24:6573–6581

Maslanik J, Drobot S, Fowler C, Emery W, Barry R (2007) On the Arctic climate paradox and the continuing role of atmospheric circulation in affecting sea ice conditions. Geophys Res Lett 34:L03711

Menary MB, Robson J, Allan RP, Booth BBB, Cassou C, Gastineau G, Gregory J, Hodsen D, Jones C, Mignot J, Ringer M, Wilcox L, Zhang R (2020) Aerosol-forced AMOC changes in CMIP6 historical simulations. Geophys Res Lett 47:e2020GL088166

Mignot J, Ganopolski A, Levermann A (2007) Atlantic subsurface temperatures: response to a shutdown of the overturning circulation and consequences for its recovery. J Clim 20:4884–4898

Muir LC, Fedorov AV (2017) Evidence of the AMOC interdecadal mode related to westward propagation of temperature anomalies in CMIP5 models. Clim Dyn 48:1517–1535

Nummelin A, Li C, Hezel PJ (2017) Connecting ocean heat transport changes from the mid-latitudes to the Arctic Ocean. Geophys Res Lett 44:1899–1908

Oldenburg D, Armour KC, Thompson L, Bitz C (2018) Distinct mechanisms of ocean heat transport into the Arctic under internal variability and climate change. Geophys Res Lett 45:7692–7700

Parkinson CL, Cavalieri DJ (2008) Arctic sea ice variability and trends, 1979–2006. J Geophys Res 113:C07003

Polyakov IV, Alekseev GV, Bekryaev RV, Bhatt US, Colony R, Johnson MA, Karklin VP, Walsh D, Yulin AV (2003) Long-term ice variability in Arctic marginal seas. J Clim 16:2078–2085

Rahmstorf S, Box JE, Feulner G, Mann ME, Robinson A, Rutherford S, Schaffernicht EJ (2015) Exceptional twentieth-century slowdown in Atlantic Ocean overturning circulation. Nat Clim Change 5:475–480

Roberts CD, Jackson L, McNeall D (2014) Is the 2004–2012 reduction of the Atlantic meridional overturning circulation significant? Geophys Res Lett 41:3204–3210

Robock A, Mao J (1992) Winter warming from large volcanic eruptions. Geophys Res Lett 19:2405–2408

Sadatzki H, Dokken TM, Berben SMP, Muschitiello F, Stein R, Fahl K, Menviel L, Timmermann A, Jansen E (2019) Sea ice variability in the southern Norwegian Sea during glacial Dansgaard-Oeschger climate cycles. Sci Adv 5:eaau6174

Schleussner CF, Feulner G (2013) A volcanically triggered regime shift in the subpolar North Atlantic Ocean as a possible origin of the Little Ice Age. Clim Past 9:1321–1330

Schweiger A, Lindsay R, Zhang J, Steele M, Stern H (2011) Uncertainty in modeled arctic sea ice volume. J Geophys Res 116:C00D06

Semenov VA, Martin T, Behrens LK, Latif M (2015) Arctic sea ice area in CMIP3 and CMIP5 climate model ensembles–variability and change. Cryosphere Discuss 9:1077–1131

Sévellec F, Fedorov AV (2013) The leading, interdecadal Eigenmode of the Atlantic meridional overturning circulation in a realistic ocean model. J Clim 26:2160–2183

Sévellec F, Fedorov AV (2015) Optimal excitation of AMOC decadal variability: links to the subpolar ocean. Prog Oceanogr 132:287–304

Sévellec F, Fedorov AV, Liu W (2017) Arctic sea-ice decline weakens the Atlantic meridional overturning circulation. Nat Clim Change 7:604–610

Shields CA, Bailey DA, Danabasoglu G, Jochum M, Kiehl JT, Levis S, Park S (2012) The low-resolution CCSM4. J Clim 25:3993–4014

Shimada K, Kamoshida T, Itoh M, Nishino S, Carmack E, McLaughlin F, Zimmermann S, Proshutinsky A (2006) Pacific Ocean inflow: influence on catastrophic reduction of sea ice cover in the Arctic Ocean. Geophys Res Lett 33:L08605

Slawinska J, Robock A (2018) Impact of volcanic eruptions on decadal to centennial fluctuations of Arctic sea ice extent during the Last Millennium and on initiation of the Little Ice Age. J Clim 31:2145–2167

Smeed DA, Josey SA, Beaulieu C, Johns WE, Moat BI, Frajka-Williams E, Rayner D, Meinen CS, Baringer MO, Bryden HL, McCarthy GD (2018) The North Atlantic Ocean is in a state of reduced overturning. Geophys Res Lett 45: 1527–1533.

Stenchikov G, Delworth TL, Ramaswamy V, Stouffer RJ, Wittenberg A, Zeng F (2009) Volcanic signals in oceans. J Geophys Res 114:D16104

Stroeve J, Holland MM, Meier W, Scambos T, Serreze M (2007) Arctic sea ice decline: faster than forecast. Geophys Res Lett 34:L09501

Sun L, Alexander M, Deser C (2018) Evolution of the global coupled climate response to Arctic Sea Ice loss during 1990–2090 and its contribution to climate change. J Clim 31:7823–7843

Swart NC, Fyfe JC, Hawkins E, Kay JE, Jahn A (2016) Influence of internal variability on Arctic sea-ice trends. Nat Clim Change 5:86–89

Swingedouw D, Ortega P, Mignot J, Guilyardi E, Masson-Delmotte V, Butler PG, Khodri M, Séférian R (2015) Bidecadal North Atlantic ocean circulation variability controlled by timing of volcanic eruptions. Nat Commun 6:6545

Swingedouw D, Mignot J, Ortega P, Khodri M, Menegoz M, Cassou C, Hanquiez V (2017) Impact of explosive volcanic eruptions on the main climate variability modes. Glob Planet Change 150:24–45

Taylor KE, Stouffer RJ, Meehl GA (2012) An overview of CMIP5 and the experiment design. Bull Am Meteorol Soc 93:485–498

Thomas MD, Fedorov AV (2019) Mechanisms and impacts of a partial AMOC recovery under enhanced freshwater forcing. Geophys Res Lett 46:3308–3316

Thornalley DJR, Oppo DW, Ortega P, Robson JI, Brierley CM, Davis R, Hall IR, Moffa-Sanchez P, Rose NL, Spooner PT, Yashayaev I, Keigwin LD (2018) Anomalously weak Labrador Sea convection and Atlantic overturning during the past 150 years. Nature 556:227–230

Titchner HA, Rayner NA (2014) The Met Office Hadley Centre sea ice and sea surface temperature data set, version 2: 1. Sea ice concentrations. J Geophys Res 119:2864–2889

Weaver AJ, Eby M, Kienast M, Saenko OA (2007) Response of the Atlantic meridional overturning circulation to increasing atmospheric CO_2: sensitivity to mean climate state. Geophys Res Lett 34:L05708

Yeager S, Karspeck A, Danabasoglu G (2015) Predicted slowdown in the rate of Atlantic sea ice loss. Geophys Res Lett 42:10704–10713

Zhang R (2010) Latitudinal dependence of Atlantic meridional overturning circulation (AMOC) variations. Geophys Res Lett 37:L16703

Zhang R (2015) Mechanisms for low-frequency variability of summer Arctic sea ice extent. Proc Natl Acad Sci 112:4570–4575

Zhang R, Vallis GK (2006) Impact of great salinity anomalies on the low-frequency variability of the North Atlantic climate. J Clim 19:470–482

Zhong Y, Miller GH, Otto-Bliesner BL, Holland MM, Bailey DA, Schneider DP, Geirsdottir A (2011) Centennial-scale climate change from decadally-paced explosive volcanism: a coupled sea ice-ocean mechanism. Clim Dyn 37:2373–2387